EEET ECOLOGICAL ENGINEERING & ENVIRONMENTAL TECHNOLOGY

Ecological Engineering & Environmental Technology, 2026, 27(10), 355–372
https://doi.org/10.12912/27197050/235670
ISSN 2719–7050, License CC-BY 4.0

Received: 2026.08.03
Accepted: 2026.09.03
Published: 2026.09.10

Urban flood modelling and evaluation of nature-based solutions at the neighbourhood scale: The case of the Tirakaa wadi, Nador (northeastern Morocco)

Hichame Sabar[1], Imad Zerhoudi[2], Maelaynayn El Baida[2], Mimoun Chourak[2], Aboubakr Chaaraoui[3], Salaheddine Amrani[4], Mostafa Oujidi[1]

[1] Laboratory of Applied Geosciences (LGA), Faculty of Science, Oujda (FSO), Mohammed I University, 60000, Oujda, Morocco
[2] Laboratory Applied Geosciences, National School of Applied Sciences of Oujda, Mohammed I University, 60000, Morocco
[3] Marchica Lagoon Site Development Agency, 62000, Nador,Morocco
[4] LaMOn2E Laboratory, Mechanics, Thermal and Energy Efficiency Research Group, Department of Physics, Faculty of Sciences, Mohammed I University, 60000 Oujda, Morocco
* Corresponding author's e-mail: h.sabar@ump.ac.ma

ABSTRACT

Urban flooding is a recurring threat in the semi-arid cities of northeastern Morocco, where urbanisation of floodplains coincides with short, intense rainfall. This study assesses the flood hazard of the Tirakaa wadi in Nador and the performance of two mitigation measures—upstream retention basins and targeted reforestation—considered separately and in combination. The 7.42 km² catchment was represented through rainfall-frequency analysis, a local intensity–duration–frequency (IDF) relationship, event-based HEC-HMS modelling with the SCS Curve Number method under average antecedent moisture conditions (AMC II; CN-II), and two-dimensional hydraulic simulation in Iber. The hourly intensity observed on 10 October 2025 (58.2 mm/h) was compared post hoc with the T100 one-hour IDF intensity (59.6 mm/h) as a single-event plausibility check, rather than as formal validation. For the T100 design-storm simulation, reforestation reduced the outlet peak discharge by 27%, the total inundated area by 2.6%, and the high-hazard area by 12.0%. On a common mapped domain, retention and the combined configuration reduced total inundated area by 5.4% and 10.2%, and high-hazard area by 7.5% and 26.3%, respectively. A complementary footprint-exclusion indicator, reported relative to the full-domain baseline, gives reductions of 21.2% and 26.0% for total inundation and 36.5% and 55.3% for high hazard when the 87,744 m² intentional-storage footprint is omitted from the basin-containing configurations. The common-domain metric provides the like-for-like comparison.

Keywords: urban flooding, nature-based solutions, HEC-HMS, Iber, retention basin, reforestation, Nador.

INTRODUCTION

Urban flooding is among the most damaging natural hazards affecting Mediterranean and semi-arid regions worldwide, causing significant loss of life and severe damage to both the natural environment and local economies. The rising frequency and intensity of flood episodes stem from the convergence of several pressures, including climate change, rapid and often unplanned urban expansion, land-use change, and the occurrence of short but intense rainfall events that exceed the limited infiltration capacity of built-up surfaces (El Baida et al., 2025; Amar et al., 2025).

In Morocco, and particularly in the eastern regions, urban flooding has become a recurring and increasingly critical challenge. The combination of unplanned urban development along natural floodplains, high variability of extreme rainfall and a semi-arid topography greatly amplifies flood risk. Recent studies in the confined basins of northeastern Morocco have revealed concerning patterns of urban encroachment and growing flood vulnerability in mountain towns (Amar et al., 2025; Afif et al., 2025; El Hadri et al., 2025).

Conventional flood-mitigation strategies have traditionally relied on grey-infrastructure solutions, including river channelisation, culverts, protective levees and detention structures. Although these approaches can provide localised protection, they are often costly, rigid and inadequate under extreme hydrometeorological conditions such as flash floods, particularly in rapidly growing urban areas. In response to these limitations, nature-based solutions (NbS) have emerged as sustainable and adaptive alternatives for flood-risk management. By restoring natural hydrological processes, namely enhanced infiltration, temporary storage and flow attenuation, NbS can provide ecological and socio-economic co-benefits, although their effectiveness remains context-dependent and important evidence gaps persist (Ruangpan et al., 2020). Mixed portfolios can balance direct flood reduction with broader co-benefits (Alves et al., 2019).

Afforestation and reforestation have been widely investigated as catchment-scale nature-based measures for flood mitigation. Increased forest cover can enhance canopy interception, improve soil permeability and increase surface roughness, thereby reducing runoff generation and delaying the flood peak. Mediterranean evidence indicates that forest effects vary with catchment size and physiography (Preti et al., 2011). Performance also depends strongly on spatial configuration, vegetation maturity and rainfall intensity, especially in semi-arid environments (Herath et al., 2025; Nadal-Romero et al., 2023).

Despite their growing adoption, nature-based solutions are not without limitations. Their flood-mitigation performance is conditioned by local soil properties, land use, spatial scale and rainfall intensity, and may decrease once infiltration or storage capacities are exceeded during extreme events (Dadson et al., 2017; Mubeen et al., 2021; Herath et al., 2025). Mediterranean modelling likewise shows that the magnitude of the benefit depends on the location and configuration of the interventions (Ferreira et al., 2020). Consequently, NbS should be integrated within flood-risk management frameworks that combine complementary green, blue and grey measures (El Baida et al., 2025; Alves et al., 2019).

While a growing body of international research addresses NbS performance at the basin and city scales (El Hadri et al., 2025), detailed neighbourhood-scale analyses focused on urban wadis remain largely absent in the Moroccan context. Against this background, the present study examines an urban catchment at the neighbourhood scale, crossed by the Tirakaa wadi in the city of Nador, northeastern Morocco. The main objective is to characterise urban flood dynamics through hydraulic modelling and to evaluate the effectiveness of nature-based solutions, specifically retention basins and targeted reforestation, in reducing flood-hazard indicators.

STUDY AREA

The Tirakaa neighbourhood lies in the northwestern part of the city of Nador, in the Oriental region of Morocco, at the interface between the Mediterranean coast and the Marchica lagoon. The Tirakaa wadi crosses the neighbourhood, where several branches and ephemeral channels (chaâbas) converge within the urban fabric before draining towards the lagoon, making Tirakaa a natural outlet for multiple upstream sub-basins (Figure 1).

Local topography is marked by a strong contrast between elevated upstream areas and low-lying downstream zones. Within the Tirakaa neighbourhood, elevations range from about 1 m near the lagoon to nearly 100 m in the western urban sectors; across the full contributing catchment, the sub-basin relief values are larger (217–605 m; Table 1). This gradient promotes rapid runoff concentration and high flow velocities during intense rainfall. Geologically, the area is part of the Nador basin, bounded to the northwest by the Gourougou volcanic massif, with an infill dominated by thick Quaternary deposits that influence surface formations and infiltration capacity.

The climate is Mediterranean with a semi-arid tendency, characterised by short but intense rainfall that is the main trigger of urban flooding. Urban development has largely followed the natural drainage network, with encroachment onto flood-prone areas. The neighbourhood is partly served by a stormwater drainage network built by the Marchica Agency; designed for frequent rainfall, this network is rapidly overwhelmed during the extreme events considered here, so that the hazard

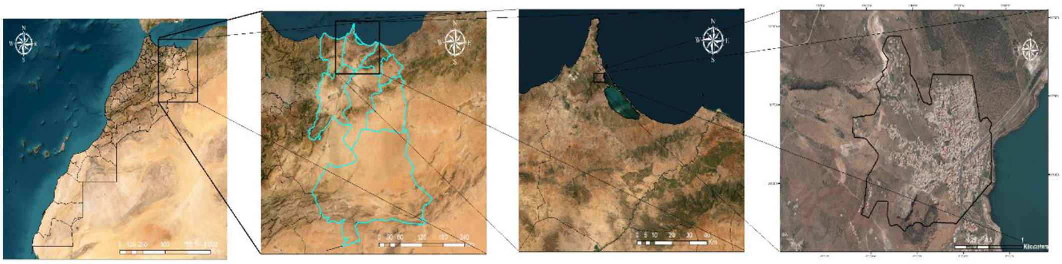

Figure 1. Location of the study area (Morocco, Oriental region, city of Nador, Tirakaa neighbourhood)

is then governed by major surface drainage. The hydraulic behaviour of the neighbourhood is further shaped by linear infrastructure: national road RN16 crosses the wadi and several chaâbas through a series of bridges and culverts, some undersized, which create hydraulic bottlenecks; and a railway embankment, running parallel to the coast, acts as a transverse barrier to drainage towards the lagoon, favouring water ponding upstream of the embankment. Finally, two abandoned sand quarries located upstream form depressions directly connected to the drainage network, potentially acting as temporary storage areas.

These hydraulic constraints result in recurring flooding at the RN16 crossing, as illustrated by the 26 January 2010 event (Figure 2), during which the culvert structure operated under pressure and the roadway was submerged.

MATERIALS AND METHODS

General methodological framework

The approach integrates spatial-data analysis, frequency analysis of extreme rainfall, event-based rainfall–runoff modelling and two-dimensional hydraulic simulation. Comparable regional studies have coupled SCS-based hydrology with two-dimensional hydraulic models for urban flood-hazard mapping (Bouiss et al., 2023; El Baida et al., 2025; Afif et al., 2025; Amar et al., 2025). These studies provide methodological precedent, not catchment-specific validation of the present parameters. The framework comprises five stages (Figure 3): (1) data collection and pre-processing; (2) frequency analysis and design storms; (3) rainfall–runoff modelling; (4) 2D hydraulic modelling and hazard mapping; and (5) evaluation of mitigation scenarios.

Data and sub-basin delineation

The digital elevation model (DEM) was derived from a photogrammetric survey carried out by the Marchica Lagoon Site Development Agency (native cell size 0.88 m, resampled to 1 m). This survey is produced for the Agency's operational needs in territorial planning and urban-planning authorisations, and therefore constitutes an engineering-grade dataset rather than a research product. It was pre-processed in GIS (ArcGIS Pro, Arc Hydro and HEC-GeoHMS) to ensure hydrological

Figure 2. Flooding of 26 January 2010 at the RN16 crossing: (a) high-velocity outflow at the five-culvert structure; (b) submersion of the RN16 roadway

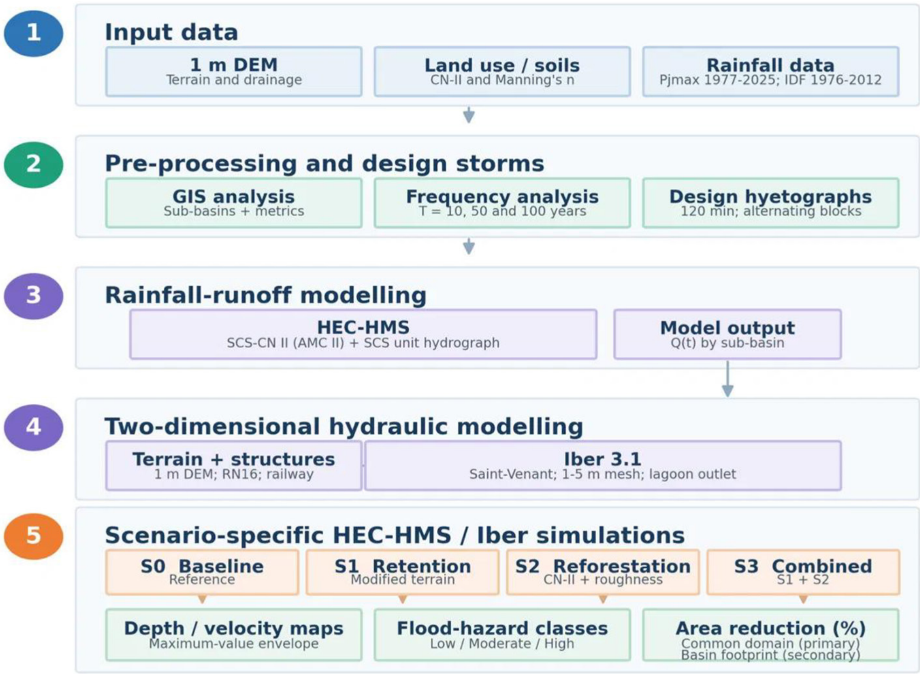

Figure 3. General methodological framework of the study

continuity of the network. The Tirakaa drainage system was subdivided into five sub-basins (SB1 to SB5), with a total area of 7.42 km² (Figure 4, Table 1). Land use (Figure 5) comprises five classes — shrubland (528.9 ha; 71.3%), residential areas (169.3 ha; 22.8%), cropland (22.9 ha), forest (12.8 ha) and bare soil (8.2 ha). Hydrological soil groups were assigned by lithological correspondence from the 1:100,000 geological map, using the formation permeabilities reported for the Gareb-Bouareg basin (Chamrar et al., 2019): Quaternary silts, gravels and sands were assigned to group B and altered volcanic rocks and marls of the Gourougou massif to group C. Groups B and C cover 28.3% and 71.7% of the catchment respectively. The land-use and soil layers were combined to derive the weighted CN-II and Manning coefficients (Supplementary Material S3).

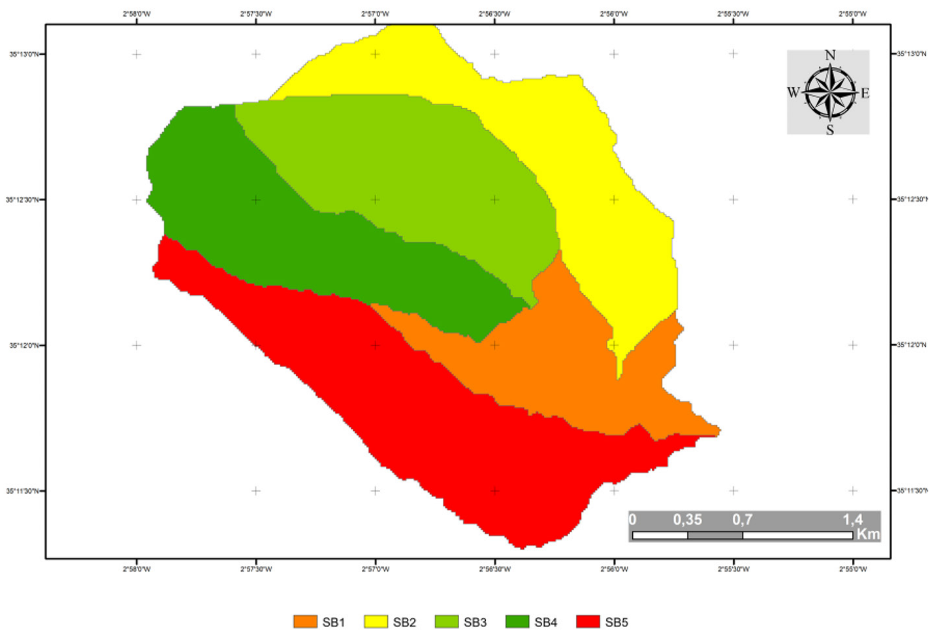

Figure 4. Delineation of the five sub-basins (SB1 to SB5) and drainage network

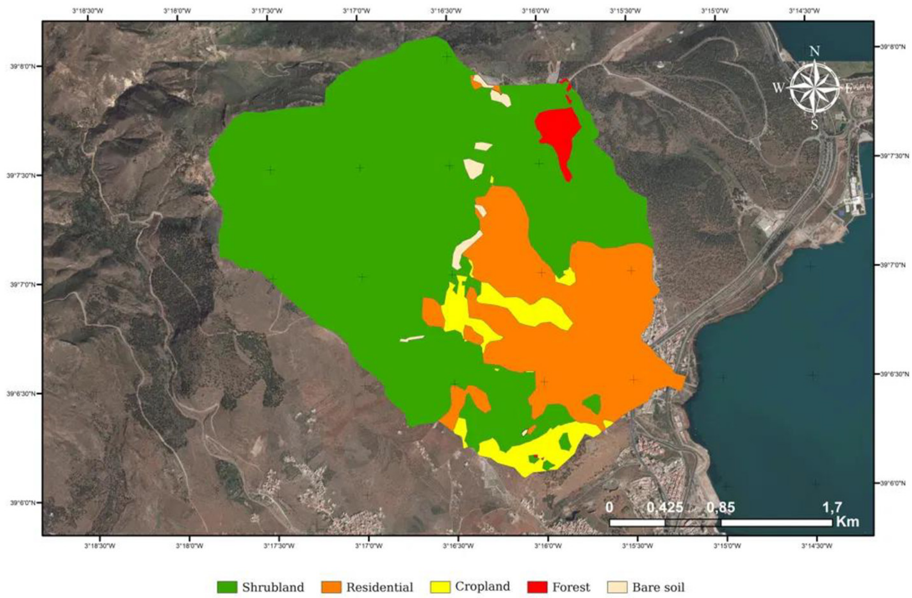

Figure 5. Land use of the Tirakaa catchment

Table 1. Morphometric characteristics of the sub-basins

Sub-basin	Area (km²)	Length (m)	ΔH (m)	Slope (m/m)	Tc (min)	Lag (min)
1	1.031	4421.1	477	0.1079	29.47	17.70
2	1.488	3985.3	516	0.1295	25.36	15.22
3	1.486	2878.6	552	0.1918	16.97	10.18
4	1.454	3077.3	605	0.1966	17.68	10.62
5	1.962	2761.2	217	0.0786	23.17	13.90
Total	7.42	—	—	—	—	—

Frequency analysis and design storm

The frequency analysis was based on the annual daily maxima (Pjmax) of the Nador-Aroui station over 1977–2025 (49 years). The annual series (Figure 6) shows strong interannual variability, with a mean of 48.1 mm and four years exceeding the ten-year threshold (85.7 mm).

The lognormal (Galton) distribution was retained after goodness-of-fit tests (Amar et al., 2025; Afif et al., 2025). The log-space parameters (μ_{ln} = 3.7231; σ_{ln} = 0.5677; n = 49) were computed from the sample mean and sample standard deviation of ln(Pjmax). Goodness-of-fit testing did not reject the lognormal model at the 5% level: the Shapiro-Wilk test applied to ln(Pjmax) gave W = 0.9843 and p = 0.7532, while the HYFRAN-PLUS chi-squared test (χ^2 = 3.35; 6 df; p = 0.764) and empirical-moment tests were also non-significant (Figure 7; Supplementary Material S4). Daily depths were converted to 24 h depths through the Weiss coefficient (P24h = 1.13 × Pjmax) (Weiss 1964) for T = 5 to 100 years (Table 2).

Because the concentration times are short (17–29 min), the design storms were derived from the local intensity–duration–frequency (IDF) relationship to represent the sub-hourly intensities governing the hydrological response (Elhassnaoui et al. 2019; El Baida et al. 2025). The IDF, described by the Montana model $i(t) = A\cdot t^{(-B)}$ (i in mm/min and t in min), was established for the Nador station over 1976–2012 (Marchica Med, 2016), with coefficients reported in Table 3. Because the design durations (≤120 min) fall within the reported fitting range (5 to approximately 745 min), the relationship was applied directly (Figure 8).

The two statistical datasets serve distinct and complementary purposes and are not combined in a single computation chain. The 1977–2025 annual daily maxima characterise the local rainfall regime and provide the return-period framework

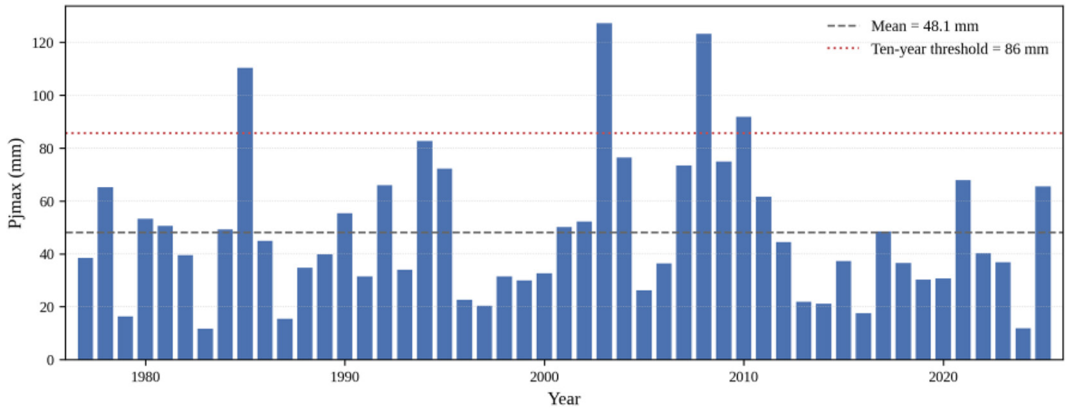

Figure 6. Annual daily maxima series (Pjmax), Nador-Aroui station (1977–2025)

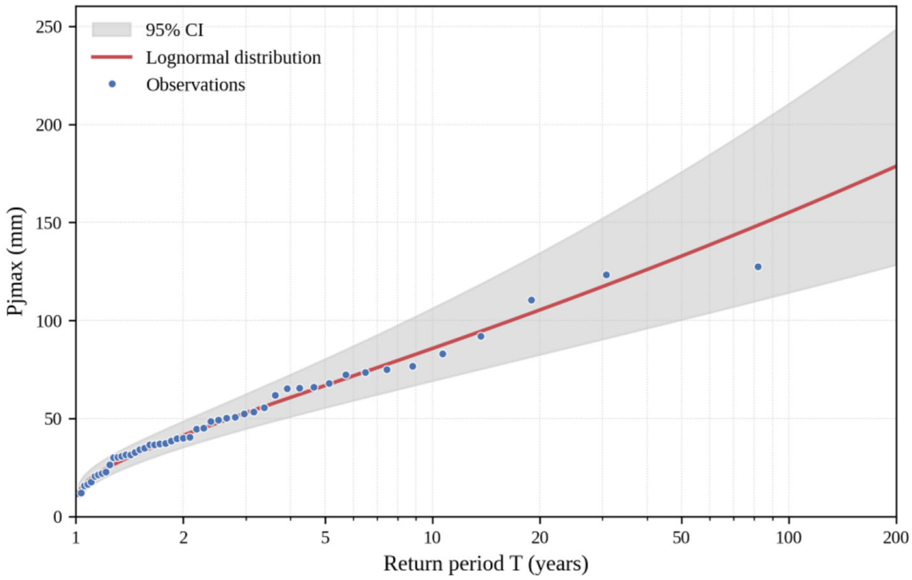

Figure 7. Lognormal fit of the Pjmax, Nador-Aroui station (1977–2025)

Table 2. Design depths from the frequency analysis

T (years)	Pjmax (mm)	95% CI lower	95% CI upper	P24h (mm)
5	66.7	54.4	79.1	75
10	85.7	67.2	104	97
20	105.3	79.5	131	119
50	132.8	95.3	170	150
100	155.0	107	203	175

Note: the 24 h depths (P24h) are reported to characterise the rainfall regime; the design storms used in the hydrological model are derived from the IDF relationship (Table 3) over 120 min.

of the study, whereas the 1976–2012 IDF relationship supplies the sub-hourly intensities required to build the design hyetographs. The two periods overlap over 1977–2012, that is 97% of the IDF fitting period, and the daily-maxima series extends it by thirteen additional years. Because the catchment response is governed by durations of 17–29 min, the design storms are derived exclusively from the IDF relationship within its calibrated sub-hourly range; the 24 h depths of Table 2 are reported to characterise the rainfall regime and are not used as input to the hydrological model. Power-law IDF models of the Montana type are fitted to short durations and should not be

Table 3. Montana coefficients of the Nador IDF (1976–2012)

T (years)	A	B
2	2.997	0.592
5	4.916	0.578
10	6.195	0.575
20	7.424	0.572
50	9.016	0.570
100	10.21	0.569

extrapolated to daily totals, which is why the two datasets are kept separate rather than merged. The agreement between the 10 October 2025 hourly observation (58.2 mm/h) and the T100 one-hour IDF intensity (59.6 mm/h), a difference of 2.4%, is treated as a single-event consistency check. It does not establish temporal stationarity or demonstrate that the 1976–2012 relationship is representative of all recent sub-hourly extremes.

The hourly intensity observed on 10 October 2025 (58.2 mm/h) is close to the T100 one-hour intensity derived from the IDF (59.6 mm/h; Figure 8). As this comparison relies on a single duration and a single event, it is treated as a consistency or plausibility check, not as statistical validation of the IDF curve. Design hyetographs were then constructed by the alternating-block method (Chow et al., 1988) for T = 10, 50 and 100 years over 120 min, using a 10-min time step (Table 4, Figure 9; Supplementary Material S1). This is a conventional synthetic temporal pattern; observed heavy storms can exhibit substantial variability in the timing of rainfall within the event (Huff, 1967).

Rainfall-runoff modelling (HEC-HMS)

The rainfall-runoff transformation was carried out with HEC-HMS (USACE, 2000). Regional studies have previously applied HEC-HMS/SCS-CN or related SCS-based workflows in northeastern Morocco (El Baida et al., 2025; Amar et al., 2025; Afif et al., 2025; Toufik et al., 2023), but they do not constitute calibration of the present catchment. In the absence of event-specific antecedent soil-moisture data, losses were estimated under average antecedent moisture conditions (AMC II), and the tabulated values are therefore denoted CN-II. The SCS relationship used Ia = 0.2S, with S = 25,400/CN-II - 254 (mm); the weighted values are reported in Table 5. The method is sensitive to the selected CN, antecedent wetness and the fixed initial-abstraction ratio (Ponce and Hawkins, 1996), while evidence from northern Morocco demonstrates the importance of antecedent wetness in event-based SCS-CN

Table 4. Total depths and peak intensities of the design hyetographs (120-min duration)

T (years)	Total depth (mm)	Peak intensity (mm/h)
10	47	99
50	71	146
100	80	165

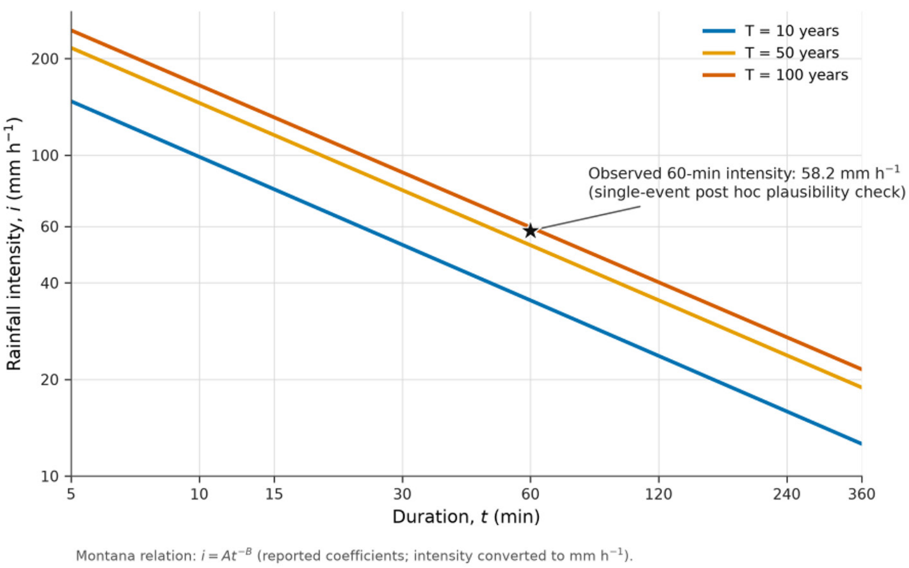

Figure 8. IDF curves for the Nador station (1976–2012) and the 10 October 2025 hourly observation used as a single-event post hoc plausibility check

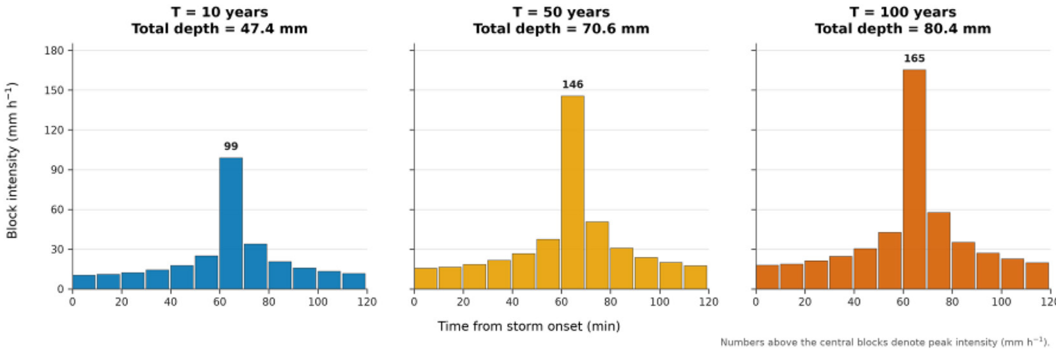

Figure 9. Alternating-block design hyetographs for T = 10, 50 and 100 years (120-min duration; 10-min blocks)

simulations (Tramblay et al., 2012). AMC II is therefore a transparent average-condition assumption rather than a calibrated catchment state. To bound the influence of CN-II and antecedent-moisture assumptions, a screening sensitivity analysis was performed for nine parameter combinations (Supplementary Material S2). Only the reference case was simulated in HEC-HMS; the other eight peak discharges were estimated from SCS-CN runoff-volume ratios and are reported as first-order bounds rather than independent simulations. Tc was estimated using Kirpich (1940), whereas basin lag was set to 0.6Tc following USDA-SCS guidance (USDA-SCS, 1972; Table 6). The resulting hydrographs supplied the upstream boundaries of the hydraulic model.

The HEC-HMS model structure comprises five sub-basin elements draining directly to a single junction, without intermediate routing reaches. This configuration reflects the physical layout of the catchment, in which the five chaâbas converge at a common confluence point immediately upstream of the modelled reach. Given the short concentration times (17–29 min) and channel lengths (2.8–4.4 km), conceptual channel routing would add limited value, and flow propagation downstream of the junction is resolved explicitly by the two-dimensional hydraulic model rather than by a lumped routing scheme. The outlet hydrograph therefore results from the superposition of the five sub-basin hydrographs at the junction, with the peak (102.9 m^3/s) slightly lower than the arithmetic sum of the individual sub-basin peaks (109.0 m^3/s) because the peaks are not simultaneous.

Table 5. SCS-CN-II loss parameters for the baseline configuration (AMC II)

Sub-basin	CN-II	S (mm)	Ia (mm)
1	77.72	72.8	14.6
2	82.62	53.4	10.7
3	84.27	47.4	9.5
4	82.38	54.3	10.9
5	78.33	70.3	14.1

Table 6. Concentration and lag times

Sub-basin	Tc Kirpich (min)	Lag = 0.6·Tc (min)
1	29.4	17.7
2	25.3	15.2
3	16.9	10.2
4	17.7	10.6
5	23.17	13.9

2D hydraulic modelling and hazard mapping (Iber)

Flood propagation was simulated with Iber 3.1, which solves the depth-averaged shallow-water (Saint-Venant) equations by a finite-volume method (Bladé et al., 2014). Unstructured finite-volume formulations are well established for overland-flow applications (Cea and Bladé, 2015). Iber has previously been applied to urban flood mapping in Morocco, including Taza and other northeastern catchments (Bouiss et al., 2023; Amar et al., 2025; Afif et al., 2025; Toufik et al., 2023); these applications provide regional precedent rather than validation of the present configuration. An unstructured mesh was generated with nominal cell sizes of 1 m along the chaâbas and 5 m elsewhere; terrain information was derived from a 1 m raster resampled from the native 0.88 m photogrammetric DEM, so that the finest mesh resolution does not exceed the raster representation used in the model. Urban inundation predictions are sensitive to computational scale and to the source and resolution of topographic data (Casas et al., 2006; Fewtrell et al., 2008). The RN16 structures and railway embankment were represented in the terrain, but no explicit building-treatment method was implemented; local velocities should therefore be interpreted cautiously because they can depend on how buildings and small-scale urban obstacles are represented (Schubert and Sanders, 2012). HEC-HMS hydrographs were imposed upstream, with a subcritical outflow condition towards the lagoon, a Courant number (CFL) of 0.15 and a wet/dry threshold of 0.01 m. Flood hazard was classified into three levels (low, moderate and high) using the depth–velocity grid in Table 7, adapted from the Annonay Flood Risk Prevention Plan (PPRI Annonay, 2010) and consistent with reviewed hazard-classification approaches (Maranzoni et al., 2023). Considering depth and velocity jointly is physically relevant because pedestrian stability depends on relative submergence and flow regime (Arrighi et al., 2017); this reference supports the combined variables, not the exact Annonay thresholds. The classification combines the maximum-depth and maximum-velocity rasters as a conservative envelope; these maxima may not occur at exactly the same simulation time.

Mitigation-scenario configurations

Two mitigation measures were evaluated separately and in combination: (i) upstream retention/detention basins, and (ii) targeted reforestation of accessible shrubland areas. All four configurations, including the baseline, were simulated on the same hydraulic computational domain using the T100 design hyetograph.

Retention basins

The retention scenario (BR) consists of three upstream basins located along the main channels of sub-basins SB2, SB3 and SB5. Two reuse abandoned sand quarries (SB3 and SB5) as temporary storage areas (Figure 10). This configuration exploits existing depressions connected to the natural drainage network. The three basin footprints cover a total of 87,744 m². Their effect was represented by local DEM modification,

Table 7. Flood hazard classification grid (depth × velocity)

Depth \ Velocity	V < 0.2 m/s	0.2 ≤ V < 0.5 m/s	V ≥ 0.5 m/s
H > 1 m	High	High	High
0.5 ≤ H ≤ 1 m	Moderate	High	High
H < 0.5 m	Low	Moderate	High

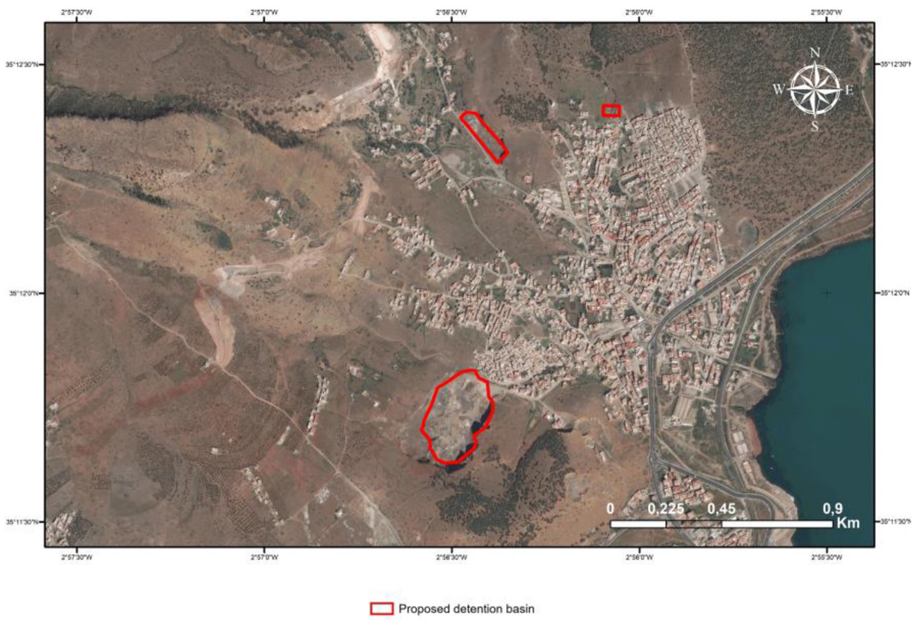

Figure 10. Location of the three proposed nature-based detention/retention basins (red outlines)

corresponding to excavation of approximately 5–5.5 m below the existing ground: bed elevations were lowered from 38 to 33 m in SB3, from 32 to 27 m in SB5, and from 31.5 to 26 m in SB2. The baseline inflow hydrographs were retained so that the hydraulic storage effect could be isolated.

Targeted reforestation

The reforestation scenario converts selected shrubland (matorral) areas to woods in fair hydrological condition. A slope-based accessibility criterion excluded terrain steeper than 30%, which was considered impractical for manual planting and maintenance (FAO 1976). This screening reduced the candidate area from 528.9 ha of total shrubland to approximately 300 ha of accessible land (57% of the shrubland), distributed unevenly among the sub-basins (Figure 11). The threshold is a planning assumption and would require field verification before implementation.

Within the selected areas, the shrubland CN-II was replaced by the value assigned to woods in fair hydrological condition (USDA-SCS 1986): from 77 to 60 for hydrological soil group B and from 85 to 73 for group C. Weighted CN-II values were recomputed for each sub-basin. In the hydraulic model, Manning's n was set to 0.10–0.12 over reforested cells to represent the increased surface roughness. These values define a prospective mature-forest scenario rather than current field conditions.

Combined scenario

The combined configuration associates the three retention basins with targeted reforestation. It therefore includes the basin-related DEM modifications, the reduced reforestation hydrographs and the higher Manning coefficients over the selected reforestation areas.

RESULTS

Rainfall–runoff response

The simulated outlet peak discharges were 34.7, 81.0 and 102.9 m³/s for the T10, T50 and T100 design storms, respectively (Table 8). For the T100 design storm, the largest sub-basin peak was obtained for SB3 (28.5 m³/s), followed by SB4 (24.8 m³/s) and SB5 (23.6 m³/s). The corresponding hydrographs are shown in Figure 12.

Baseline hydraulic hazard

For the baseline T100 design-storm simulation, the simulated maximum water depth reached 1.96 m and the maximum velocity reached 7.9 m/s (Figures 13 and 14). High-hazard cells were concentrated along the chaâbas, at channel confluences and near the downstream RN16 and railway structures (Figure 15). The maximum velocity occurs on upstream hillslope cells where the local

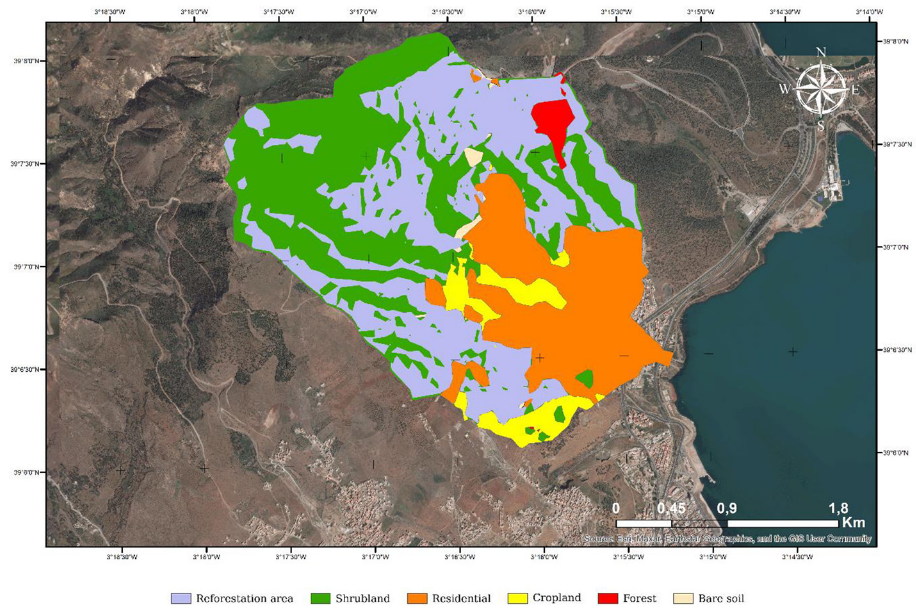

Figure 11. Accessible shrubland areas selected for reforestation (lavender), after applying the <30% slope criterion

Table 8. Simulated peak discharges – baseline (m³/s)

Sub-basin	T = 10 years	T = 50 years	T = 100 years
1	3.1	8.6	10.6
2	7.6	17.1	21.5
3	7.5	22.9	28.5
4	8.2	19.7	24.8
5	7.0	18.2	23.6
Outlet	34.7	81.0	102.9

terrain gradient reaches 56% (29.4°). At that location the simulated depth is 0.21 m and the Froude number is 4.7, indicating a supercritical torrential regime. The velocity is consistent with the Manning formulation for the assigned slope and roughness, and is therefore a physically admissible solution rather than a numerical artefact; however, natural rock-step and boulder roughness that dissipates energy on such slopes is not resolved at the

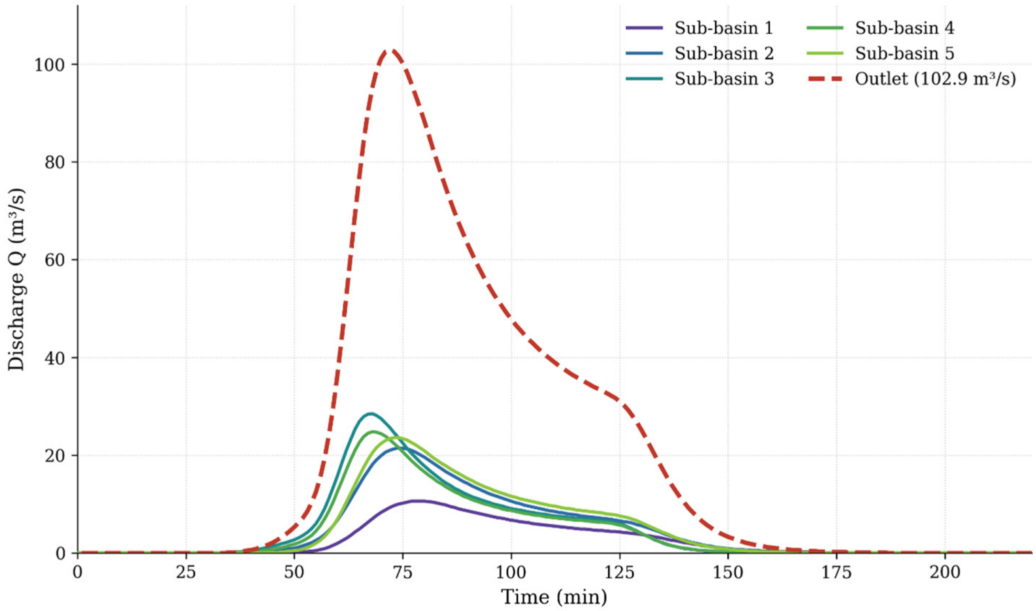

Figure 12. Flood hydrographs for the five sub-basins and at the outlet under the baseline T100 design storm

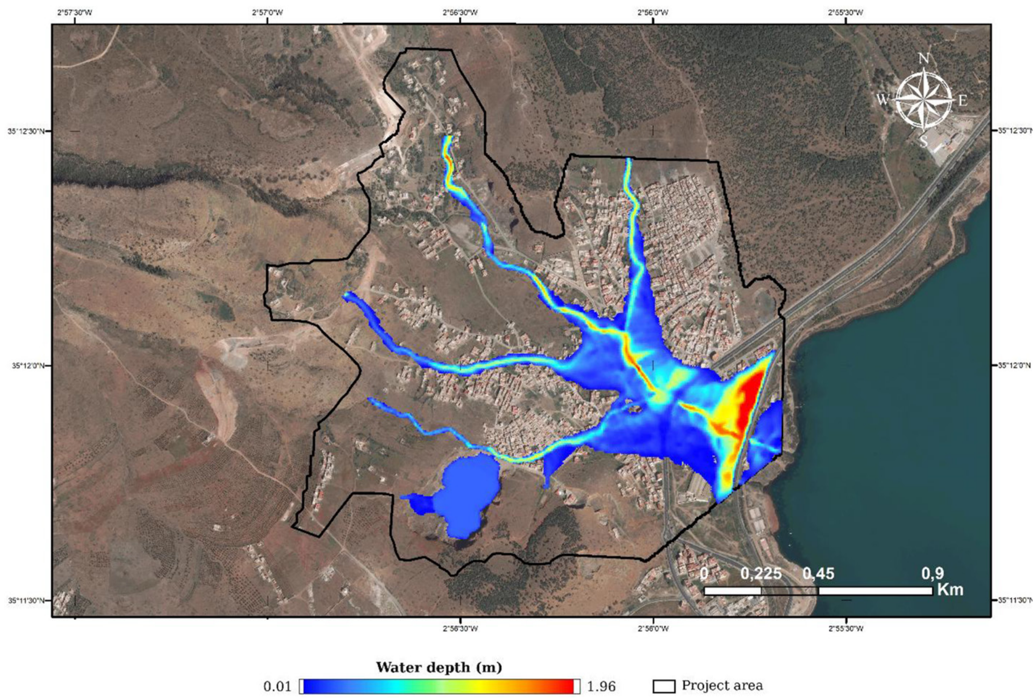

Figure 13. Maximum simulated water depth for the baseline T100 design-storm simulation

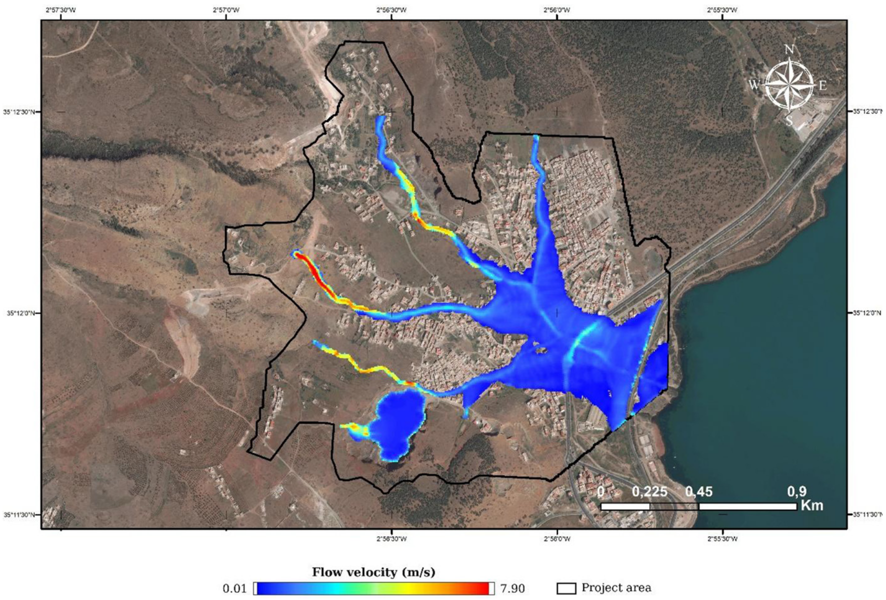

Figure 14. Maximum simulated flow velocity for the baseline T100 design-storm simulation

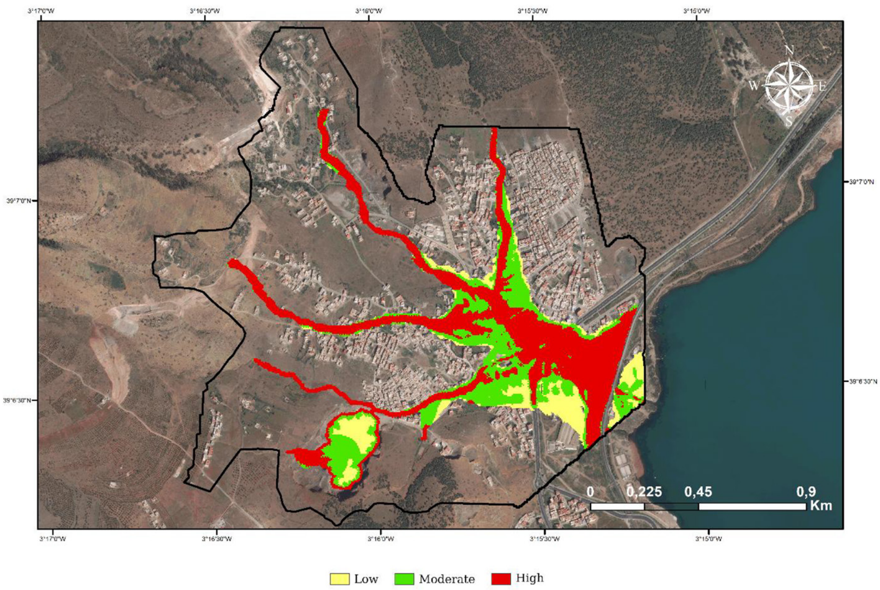

Figure 15. Flood-hazard map for the baseline T100 design-storm simulation

model scale, so these peak values are likely to be overestimated. They occur in the upper catchment, outside the urbanised sectors where the hazard assessment is targeted, and are not used to support any conclusion about urban exposure.

Performance of the mitigation configurations

Retention basins

With the baseline inflows unchanged, the excavated basins redirected water into the designated upstream storage areas and reduced downstream hazard (Figure 16). Because stored water is intentionally mapped within the basin footprints.

Targeted reforestation

Reforestation reduced the T100 outlet peak from 102.9 to 75.0 m³/s (27.1%) and the T10 peak by 42.4% (Table 9; Figure 17). In the hydraulic results, total inundated area decreased by 2.6% and high-hazard area by 12.0%, whereas low-hazard area increased. These are aggregate class changes; a cell-by-cell transition matrix was not calculated (Figure 18).

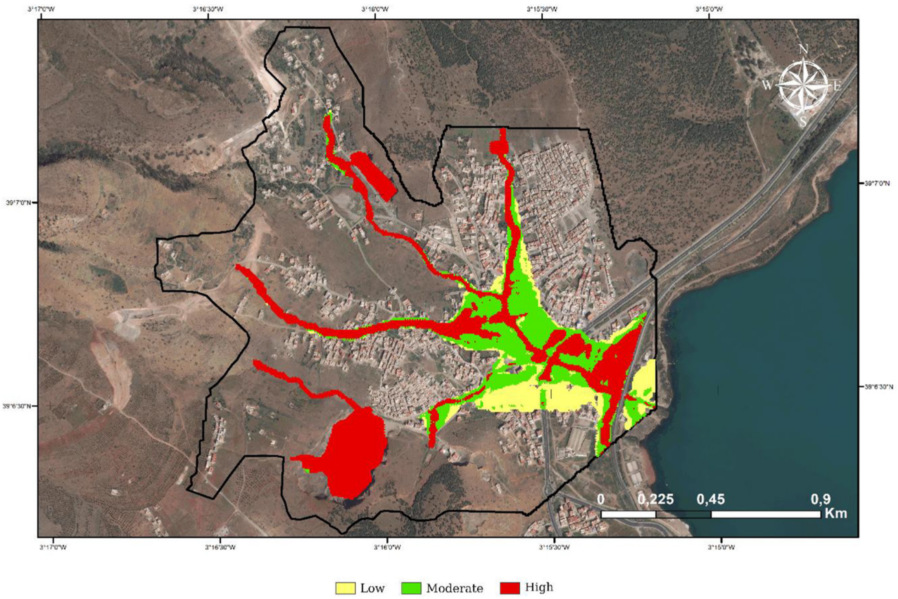

Figure 16. Flood-hazard map for the retention-basin configuration (T100 design storm)

Table 9. Targeted reforestation: weighted CN and hundred-year peak discharges per sub-basin

Sub-basin	Baseline CN-II	Reforested CN-II	Qp T100 baseline (m³/s)	Qp T100 reforested (m³/s)
1	77.72	77.00	10.6	10.2
2	82.62	77.33	21.5	16.1
3	84.27	78.39	28.5	20.7
4	82.38	75.62	24.8	16.8
5	78.33	71.79	23.6	15.6
Outlet	—	—	102.9	75.0

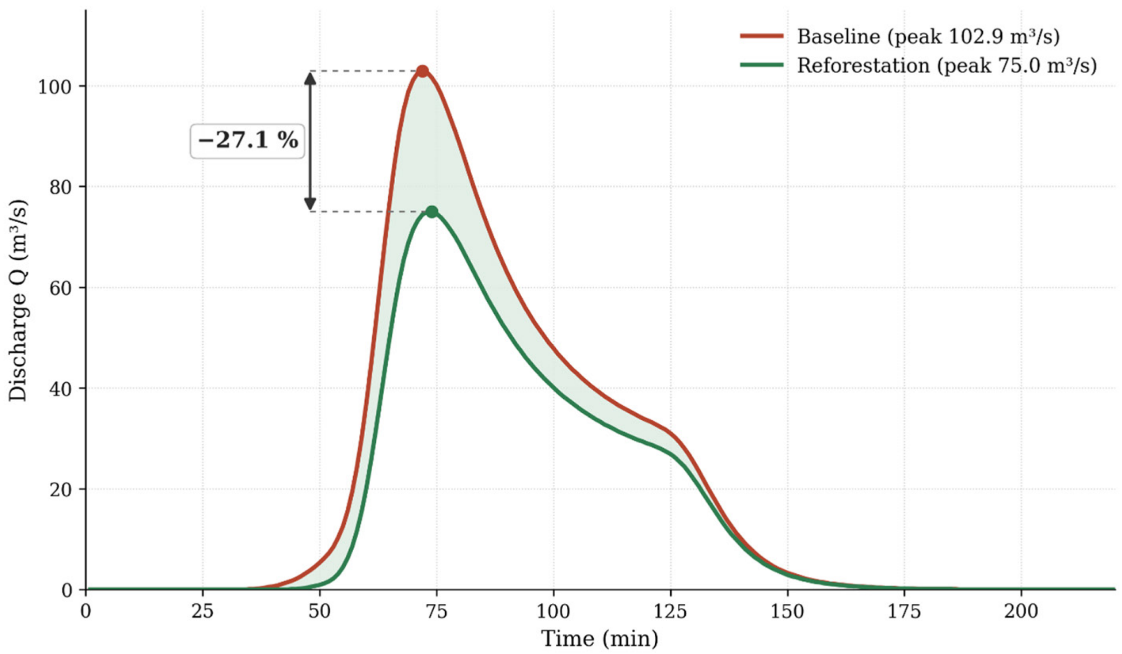

Figure 17. T100 outlet hydrograph: baseline and reforestation configuration under fair forest condition

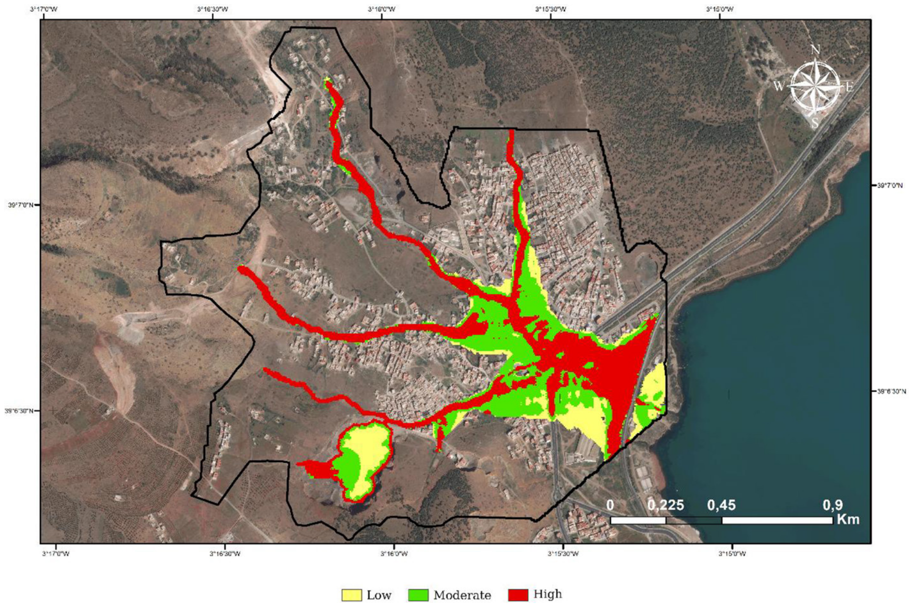

Figure 18. Flood-hazard map for the targeted-reforestation configuration (T100 design storm)

Combined configuration

The combined configuration produced the smallest high-hazard footprint among the four mapped configurations (Figure 19).

Cross-scenario comparison

All simulations used the same hydraulic computational domain, but two post-processing indicators are reported to make the treatment of intentional storage explicit (Table 10; Figure 20). The common mapped-domain comparison includes every wet cell, including the basin cells, which are classified as high hazard because they contain intentionally stored water. Adding the 87,744 m² storage footprint back to the reported retention and combined totals gives like-for-like reductions of 5.4% and 10.2% in total inundated area and 7.5% and 26.3% in high-hazard area, respectively. Reforestation reduced total inundated area by 2.6% and high-hazard area by 12.0%. For

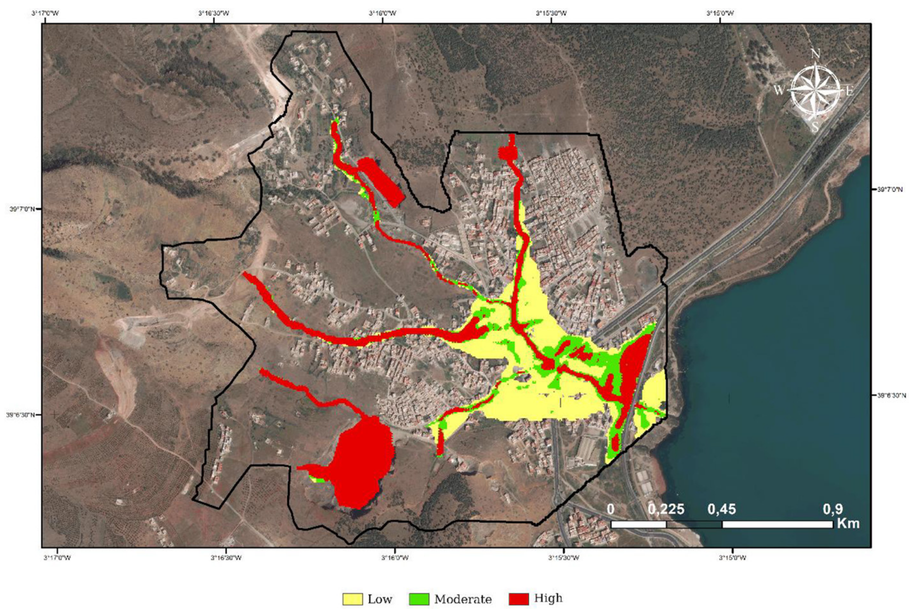

Figure 19. Flood-hazard map for the combined retention-basin and reforestation configuration (T100 design storm)

Table 10. Percentage reduction relative to baseline for the T100 design-storm simulation under two spatial accounting metrics

Configuration	Common domain Total (%)	Common domain High (%)	Footprint-excluded* Total (%)	Footprint-excluded* High (%)
Retention	5.4	7.5	21.2	36.5
Reforestation	2.6	12.0	—	—
Combined	10.2	26.3	26.0	55.3

Note : *the footprint-exclusion indicator is reported relative to the full-domain baseline; it omits the 87,744 m² storage footprint from the retention and combined configurations only and is therefore not a like-for-like spatial comparison.

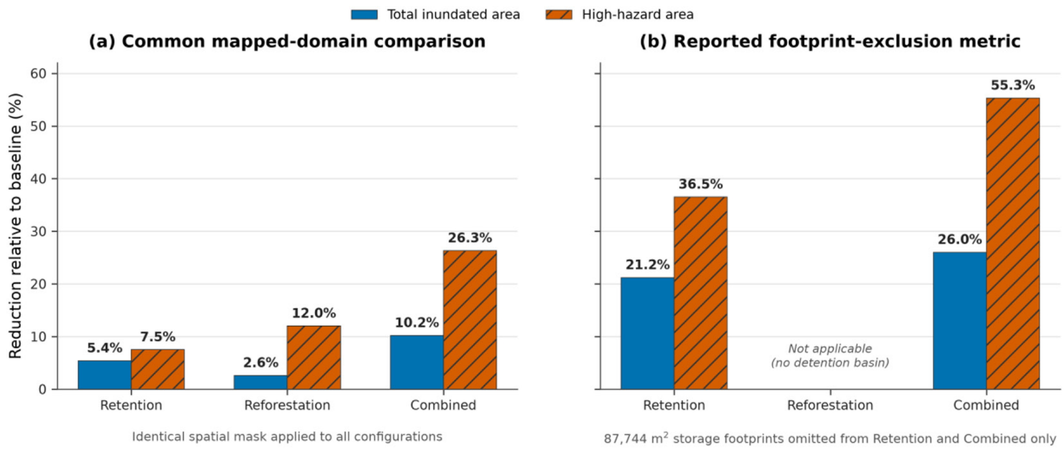

Figure 20. Percentage reductions relative to baseline under (a) common mapped-domain accounting and (b) the footprint-exclusion indicator omitting the 87,744 m² storage footprint from the retention and combined configurations only

continuity with the initial reporting, a secondary footprint-exclusion indicator is also retained: the 87,744 m² footprint is omitted from the retention and combined configurations, but the full-domain baseline remains the denominator. It yields 21.2% and 36.5% for retention and 26.0% and 55.3% for the combined configuration. Because that second indicator does not use a common spatial mask, it is descriptive and must not be interpreted as an off-site reduction. The common-domain values provide the principal comparison.

DISCUSSION

This study characterised the flood hazard of the Tirakaa neighbourhood and evaluated two mitigation measures separately and in combination. The coupled HEC-HMS/Iber simulation forced by the T100 design hyetograph indicates an extensive high-hazard zone along the chaâbas and near the downstream RN16 and railway structures, with maximum mapped depths and velocities of 1.96 m and 7.9 m/s. On the common mapped domain, the combined configuration gave the largest reduction: 10.2% of total inundated area and 26.3% of high-hazard area. The larger values obtained with the footprint-exclusion indicator (26.0% and 55.3%) partly reflect omission of the intentional-storage footprint and are therefore reported only as a secondary descriptive metric.

The 10 October 2025 hourly observation was compared post hoc with the adopted IDF relationship. Its intensity of 58.2 mm/h is close to the T100 one-hour IDF value of 59.6 mm/h. This single-event comparison is useful as a plausibility check, but it cannot validate an entire IDF curve or its return-period assignment. The design storms therefore remain based on the 1976–2012 local IDF relationship and should be interpreted in light of uncertainty in that IDF fit and in the separate 49-year daily-maximum analysis.

The two measures affect different model components. Retention basins modify terrain storage, whereas reforestation changes the assumed SCS loss and surface-roughness parameters. They should therefore be interpreted as complementary rather than interchangeable. Mediterranean modelling indicates that strategically located storage and land-cover measures can attenuate flood response, but their combined effect remains site- and event-specific (Ferreira et al., 2020). This portfolio perspective is consistent with work showing that mixed infrastructure strategies can balance direct flood reduction with wider co-benefits (Alves et al., 2019). The reforestation scenario reduced high-hazard area more than total inundated area. The difference between the common-domain and footprint-exclusion indicators is substantial and shows why intentional-storage cells must be identified explicitly instead of being silently removed from only some scenario totals.

The decline in the modelled relative discharge reduction from 42% for T10 to 30% for T50 and 27% for T100 is consistent with the generally reduced relative effectiveness of infiltration-based measures during more extreme events (Herath et al., 2025; Nadal-Romero et al., 2023). Regional studies have also evaluated storage and land-management measures (El Baida et al., 2025; Afif et al., 2025). These comparisons provide context for the simulated tendencies, not independent validation of the Tirakaa parameterisation.

From an operational standpoint, reusing existing quarry depressions may reduce excavation requirements, while the slope screening identifies a practicable first estimate of accessible reforestation land. Both remain conceptual planning scenarios: basin stage–storage curves, inlet/outlet and overflow structures, geotechnical safety, land tenure, vegetation species and establishment time would need site-specific design before implementation.

Several limitations should be noted. No observed discharge hydrographs or surveyed inundation extents were available for quantitative calibration of HEC-HMS or Iber; the cited regional studies provide methodological precedent only. Multi-event calibration and verification would better constrain event-based HEC-HMS parameters (Chu and Steinman, 2009), while equifinality supports formal sensitivity and uncertainty analysis rather than reliance on a single plausible parameter set (Beven and Binley, 1992). CN-II and Manning values remain scenario assumptions. The 1 m channel mesh matches the native resolution of the DEM, so the mesh does not extrapolate beyond the available terrain information; the model does not, however, resolve individual buildings. The downstream lagoon level was represented by a simplified subcritical outflow condition, which may omit backwater and compound effects associated with the interaction of river discharge and downstream water levels in coastal environments (Kumbier et al., 2018). Finally, the 0.01 m wet/dry threshold and the use of maximum depth and velocity as a conservative envelope influence mapped hazard extents. The dual spatial accounting used here makes the 87,744 m² storage-footprint effect transparent.

In the absence of gauged discharges, surveyed flood marks or mapped inundation extents, no quantitative calibration or validation of either the hydrological or the hydraulic model was possible for this catchment. The photographic record of the January 2010 event documents the occurrence and location of flooding at the RN16 crossing but does not provide measured depths or velocities. The results presented here should therefore be interpreted as scenario modelling of the relative differences between configurations, rather than as a verified assessment of absolute flood hazard. The relative rankings between mitigation configurations are more robust than the absolute values, since all configurations share the same parameterisation, forcing and computational domain.

Future work should compare simulated hydrographs and inundation patterns with event observations, extend the screening sensitivity analysis through full HEC-HMS and Iber reruns, and evaluate the effects of CN-II, Manning's n, the wet/dry threshold, mesh resolution and lagoon level. Basin stage-storage-outflow behaviour should also be represented explicitly. Coupling Iber with a drainage-network model such as SWMM would also improve representation of interactions between surface flow and the partial stormwater network, including the hydraulic connectivity beneath the railway embankment.

CONCLUSIONS

This study characterised the flood hazard of the Tirakaa neighbourhood and evaluated two mitigation measures—upstream retention basins and targeted reforestation—separately and in combination. In the simulation forced by the T100 design hyetograph, high hazard was concentrated along the chaâbas and near the downstream transport infrastructure.

The 10 October 2025 hourly intensity provides a single-event post hoc plausibility check on the local IDF relationship, but not formal validation. Reforestation reduced the modelled T100 outlet peak by 27%, total inundated area by 2.6% and high-hazard area by 12.0%. On the common mapped domain, retention and the combined configuration reduced total inundation by 5.4% and 10.2%, and high hazard by 7.5% and 26.3%. The complementary footprint-exclusion indicator gives larger reductions of 21.2% and 26.0% in total inundation and 36.5% and 55.3% in high hazard; because it omits the 87,744 m² storage footprint only from basin-containing configurations, it is retained for continuity but is not the principal like-for-like comparison.

The results support further investigation of quarry-based temporary storage and targeted reforestation as complementary measures. Their feasibility and performance should be confirmed through field surveys, event-based calibration, full simulation-based sensitivity analysis, explicit basin-outlet design and representation of the stormwater network and lagoon boundary.

REFERENCES

1. Afif H, Oujidi M, Chourak M, Amar I, Ramdani S (2025) Assessment of flood hazards in Greater Berkane for the selection of nature-based solutions, Oriental region, Morocco. *Model Earth Syst Environ 11*:139. https://doi.org/10.1007/s40808-025-02332-z
2. Alves A, Gersonius B, Kapelan Z, Vojinovic Z, Sanchez A (2019) Assessing the co-benefits of green-blue-grey infrastructure for sustainable urban flood risk management. *J Environ Manage 239*:244–254. https://doi.org/10.1016/j.jenvman.2019.03.036
3. Amar I, Bengamra S, Chourak M, Jilali A, Afif H, Bouiss H, Sabar H, Ramdani S (2025) 2D modeling and flood hazard mapping of the El-Hai and Msakhshka rivers in the city of Ain Beni Mathar (NE Morocco). *Model Earth Syst Environ 11*:263. https://doi.org/10.1007/s40808-025-02439-3
4. Arrighi C, Oumeraci H, Castelli F (2017) Hydrodynamics of pedestrians' instability in floodwaters. *Hydrol Earth Syst Sci 21*:515–531. https://doi.org/10.5194/hess-21-515-2017
5. Beven K, Binley A (1992) The future of distributed models: model calibration and uncertainty prediction. *Hydrol Process 6*(3):279–298. https://doi.org/10.1002/hyp.3360060305
6. Bladé E, Cea L, Corestein G, Escolano E, Puertas J, Vázquez-Cendón E, Dolz J, Coll A (2014) Iber: herramienta de simulación numérica del flujo en ríos. *Rev Int Métodos Numér Cálc Diseño Ing 30*(1):1–10. https://doi.org/10.1016/j.rimni.2012.07.004
7. Bouiss H, Bengamra S, Amarjouf N, Oujidi M, Amar I, Grari A (2023) Application of two-dimensional hydraulic modelling of hydrological risk related to urban flood: a case of Taza City, Morocco. *Ecol Eng Environ Technol 24*(6):173–185. https://doi.org/10.12912/27197050/168332
8. Casas A, Benito G, Thorndycraft VR, Rico M (2006) The topographic data source of digital terrain models as a key element in the accuracy of hydraulic flood modelling. *Earth Surf Process Landf 31*(4):444–456. https://doi.org/10.1002/esp.1278
9. Cea L, Bladé E (2015) A simple and efficient unstructured finite volume scheme for solving the shallow water equations in overland flow applications. *Water Resour Res 51*(7):5464–5486. https://doi.org/10.1002/2014WR016547
10. Chamrar A, Oujidi M, El Mandour A, Jilali A (2019) 3D geological modeling of Gareb-Bouareg basin in northeast Morocco. *J Afr Earth Sci 154*:172–180. https://doi.org/10.1016/j.jafrearsci.2019.03.023
11. Chow VT, Maidment DR, Mays LW (1988) *Applied hydrology.* McGraw-Hill, New York
12. Chu X, Steinman A (2009) Event and continuous hydrologic modeling with HEC-HMS. *J Irrig Drain Eng 135*(1):119–124. https://doi.org/10.1061/(ASCE)0733-9437(2009)135:1(119)
13. Dadson SJ, Hall JW, Murgatroyd A, Acreman M, Bates P, Beven K, Heathwaite L, Holden J, Holman IP, Lane SN, O'Connell E, Penning-Rowsell E, Reynard N, Sear D, Thorne C, Wilby R (2017) A restatement of the natural science evidence concerning catchment-based 'natural' flood management in the UK. *Proc R Soc A 473*(2199):20160706. https://doi.org/10.1098/rspa.2016.0706
14. El Baida M, Chourak M, Boushaba F (2025) Flood mitigation and water resource preservation: hydrodynamic and SWMM simulations of nature-based solutions under climate change. *Water Resour Manag 39*(3):1149–1176. https://doi.org/10.1007/s11269-024-04015-3
15. El Hadri L, Boushaba F, Chourak M, El Baida M (2025) Mapping flood hazard in Driouch region (north-eastern of Morocco) using AHP and numerical approaches. *J Afr Earth Sci 231*:105776. https://doi.org/10.1016/j.jafrearsci.2025.105776
16. Elhassnaoui I, Moumen Z, Bouziane A, Ouazar D, Hasnaoui MD (2019) Generation of synthetic design storm hyetograph and hydrologic modeling under HEC-HMS for Ziz watershed. *Int J Innov Technol Explor Eng 8*(10):3308–3319. https://doi.org/10.35940/ijitee.j1214.0881019
17. FAO (1976) A framework for land evaluation. FAO Soils Bulletin 32. *Food and Agriculture Organization of the United Nations, Rome.*

18. Ferreira CSS, Mourato S, Kasanin-Grubin M, Ferreira AJD, Destouni G, Kalantari Z (2020) Effectiveness of nature-based solutions in mitigating flood hazard in a Mediterranean peri-urban catchment. *Water 12*(10):2893. https://doi.org/10.3390/w12102893
19. Fewtrell TJ, Bates PD, Horritt M, Hunter NM (2008) Evaluating the effect of scale in flood inundation modelling in urban environments. *Hydrol Process 22*(26):5107–5118. https://doi.org/10.1002/hyp.7148
20. Herath P, Croke B, Prinsley R, Vaze J, Pollino C (2025) A systematic review of forest cover for catchment-scale flood mitigation: a nature-based solution. *J Flood Risk Manag.* https://doi.org/10.1111/jfr3.70125
21. Huff FA (1967) Time distribution of rainfall in heavy storms. *Water Resour Res 3*(4):1007–1019. https://doi.org/10.1029/WR003i004p01007
22. Kirpich ZP (1940) Time of concentration of small agricultural watersheds. *Civ Eng 10*(6):362.
23. Kumbier K, Carvalho RC, Vafeidis AT, Woodroffe CD (2018) Investigating compound flooding in an estuary using hydrodynamic modelling: a case study from the Shoalhaven River, Australia. *Nat Hazards Earth Syst Sci 18*:463–477. https://doi.org/10.5194/nhess-18-463-2018
24. Maranzoni A, D'Oria M, Rizzo C (2023) Quantitative flood hazard assessment methods: a review. *J Flood Risk Manag 16*(1):e12855. https://doi.org/10.1111/jfr3.12855
25. Marchica Med (2016) Réalisation d'un diagnostic et études de protection du site de la lagune de Marchica contre les inondations. *Agence pour l'Aménagement du Site de la Lagune de Marchica, Nador*
26. Mubeen A, Ruangpan L, Vojinovic Z, Sanchez Torrez A, Plavšić J (2021) Planning and suitability assessment of large-scale nature-based solutions for flood-risk reduction. *Water Resour Manag 35*:3063–3081. https://doi.org/10.1007/s11269-021-02848-w
27. Nadal-Romero E, Llena M, Cortijos-López M, Lasanta T (2023) Afforestation after land abandonment as a nature-based solution in Mediterranean mid-mountain areas: implications and research gaps. *Curr Res Environ Sustain*. https://www.sciencedirect.com/science/article/pii/S2468584423000417
28. Ponce VM, Hawkins RH (1996) Runoff curve number: has it reached maturity? *J Hydrol Eng 1*(1):11–19. https://doi.org/10.1061/(ASCE)1084-0699(1996)1:1(11)
29. PPRI Annonay (2010) Plan de prévention des risques d'inondation de la commune d'Annonay. *Préfecture de l'Ardèche, France*
30. Preti F, Forzieri G, Chirico GB (2011) Forest cover influence on regional flood frequency assessment in Mediterranean catchments. *Hydrol Earth Syst Sci 15*:3077–3090. https://doi.org/10.5194/hess-15-3077-2011
31. Ruangpan L, Vojinovic Z, Di Sabatino S, Leo LS, Capobianco V, Oen AMP, McClain ME, Lopez-Gunn E (2020) Nature-based solutions for hydro-meteorological risk reduction: a state-of-the-art review of the research area. *Nat Hazards Earth Syst Sci 20*:243–270. https://doi.org/10.5194/nhess-20-243-2020
32. Schubert JE, Sanders BF (2012) Building treatments for urban flood inundation models and implications for predictive skill and modeling efficiency. *Adv Water Resour 41*:49–64. https://doi.org/10.1016/j.advwatres.2012.02.012
33. Toufik Z, Sabar H, Farid B, Chourak M (2023) Mapping the risk of flooding of the national road N°2 at the crossing of the wadi Tamdmadt north of the city of Bni Drar. *Mater Today Proc 72*:3447–3453. https://doi.org/10.1016/j.matpr.2022.08.089
34. Tramblay Y, Bouaicha R, Brocca L, Dorigo W, Bouvier C, Camici S, Servat E (2012) Estimation of antecedent wetness conditions for flood modelling in northern Morocco. *Hydrol Earth Syst Sci 16*:4375–4386. https://doi.org/10.5194/hess-16-4375-2012
35. USACE (2000) Hydrologic modeling system HEC-HMS technical reference manual. US Army Corps of Engineers, Hydrologic Engineering Center, Davis
36. USDA-SCS (1972) National Engineering Handbook, Section 4: Hydrology. US Department of Agriculture, Soil Conservation Service, Washington DC
37. Weiss LL (1964) Ratio of true to fixed-interval maximum rainfall. *J Hydraul Div 90*(1):77–82. https://doi.org/10.1061/JYCEAJ.0001008